JOURNAL OF EXPERIMENTAL AND THEORETICAL PHYSICS, 2024, Vol. 165, No. 3, pp. 427–439

SOLID BODIES ELECTRONIC PROPERTIES

REGIMES OF ELECTRONIC TRANSPORT IN DOPED InAs NANOWIRE

© 2024 A. A. Zhukov [a*], I. E. Batov [a,b]

[a] Osipyan Institute of Solid State Physics RAS, Chernogolovka, 142432, Russia
[b] Faculty of Physics, National Research University Higher School of Economics, Moscow 101000, Russia
*e-mail: azhukov@issp.ac.ru

Received July 28, 2023
Revised October 29, 2023
Accepted October 30, 2023

Abstract. We report on the low temperature measurements of the magnetotransport in Si-doped InAs quantum wire in the presence of a charged tip of an atomic force microscope serving as a mobile gate, i.e. scanning gate microscopy (SGM). By altering the carrier concentration with back gate voltage, we transfer the wire through several transport regimes: from residual Coulomb blockade to nonlinear resonance regime, followed by linear resonance regime and, finally, to almost homogeneous diffusion regime. We demonstrate direct relations between patterns measured with scanning gate microscopy and spectra of universal conductance fluctuations in the dependence of conductance on magnetic field ($R^{-1}(B)$). Additionally, a clear sign of fractal behavior of $R^{-1}(B)$ curve is observed for non-linear and linear resonance transport regimes.

Keywords: *Scanning gate microscopy*, *semiconducting nanowires*, *mesoscopics*

DOI: 10.31857/S00444510240312e7

1. INTRODUCTION

One of the peculiarities of one-dimensional and quasi-one-dimensional diffusion electronic transport is the presence in these type of systems an electron scattering from so-called resonance scatterers. These scatterers, such as weak links or any other potential barriers, influence on electrons in all channels. If these scatterers are strong enough and temperature T is low, the transport can demonstrate Coulomb blockade [1] ($h/\tau, k_B T < e^2/c$) or zero-bias anomaly [2], here h — is Planck's constant, k_B is Boltzmann's constant, τ is the tunneling time through barriers, e is elementary charge and c is capacitance of the system section in between two nearest weak links. In the case that potential barriers are weak, the transport is linear but well-defined resonances in magnetoresistance can be observed due to over-barrier reflections [3]. Finally, if the role of such barriers/scatterers is negligible, the homogeneous diffusive transport regime is realized [4].

In samples with the phase coherence length (l_ϕ) of the charge carriers (the distance the electron travels before its phase is randomized) comparable to the sample size (l_{wire}), the universal conductance fluctuations (UCF) are observed [5].

Using the correlator

$$F(\Delta B) = \left\langle \delta R^{-1}(B) \delta R^{-1}(B + \Delta B) \right\rangle,$$
$$\delta R^{-1}(B) = \left\langle R^{-1} \right\rangle - R^{-1}(B),$$

it is possible to extract the value of

$$l_\phi = \Phi_0 / dB_c.$$

from the correlation field B_c defined as $F(B_c) = 0.5F(0)$ [6, 7], $\Phi_0 = e/h$ is the quantum flux and d is a constant of the order of unity [7]. According to the work [8], the deviation of correlation function is

$$\Delta F(\Delta B) = F(0) - F(\Delta B) \propto \Delta B^\gamma,$$

and the value of exponent γ defines the dimension of the fractional Brownian motion $D = 2 - \gamma/2$ [9-11] of dependence of conductance on magnetic

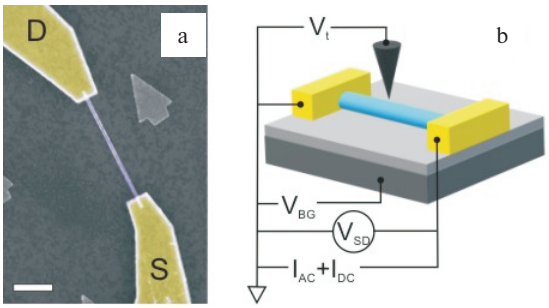

Fig. 1. (In color online) a) False color scanning electron microscope image of the sample nanowire. The scale bar corresponds to 1μm. b) Schematic diagram of the experimental setup. In the Figures, the nanowire has a blue color and two metallic contact pads are yellow, source and drain contacts are labelled as S and D, respectively

field $R^{-1}(B)$. Fractional Brownian motion has been found in quasiballistic Au-nanowires [12], different types of semiconductor nanowires [13], and graphene stripes [14].

Here, we present a detailed investigation of magnetotransport in Si-doped InAs nanowire using SGM mapping and standard magnetotransport measurements in a wide range of carrier concentrations. The system passed through four transport regimes from residual Coulomb blockade to non-linear resonance scattering, then to linear resonance scattering and finally to quasi-homogenious diffusion regime. The role of resonant scatterers in formation of fractional Brownian motion of $R^{-1}(B)$ curve is discussed.

2. EXPERIMENTAL

The nanowires were grown on GaAs (111) substrates by low-pressure metal organic vapor phase epitaxy (MOVPE). Nitrogen gas (N_2) was used as the carrier gas to transport trimethylindium ($In(CH_3)_3$) and arsine (AsH_3) in the reactor at a working pressure of 20 mbar and a total gas flow rate of 3100 ml/min. The growth temperature was 650 ° C. For silicon doping during growth, the disilane (Si_2H_6) flux was adjusted to achieve various *n*-type doping levels. To quantify the supply of doping species more easily, doping factor, consisting of the partial pressure ratio of dopant versus group III precursor, is defined as a ratio of $p(Si_2H_6)/p(In(CH_3)_3)$. The ratio of $7.5 \cdot 10^{-4}$ was used for growth the batch of the nanowires investigated in the current experiment. Additional details of the Si-doped nanowires growth procedure can be found elsewhere [15,16].

The diameter of the wire was $d_{wire} = 100$ nm. The wire was placed on an *n*-type doped Si(100) substrate covered by a thermal grown 100 nm thick SiO_2 insulating layer. The Si substrate served as the back-gate electrode. The Ti/ Au - contacts to the wire as well as the markers of the search pattern were defined by electron beam lithography. The distance between the contacts was $l_{wire} = 2.9$ μm. A scanning electron beam micrograph of the sample is shown in Fig. la). The source and drain metallic electrodes connected to the wire are marked as S and D.

All measurements were performed at $T = 4.2$ K. The charged tungsten tip of a home-built scanning probe microscope [17] was used as a mobile gate during scanning gate imaging measurements, see Fig. 1b). All scanning gate measurements were performed by keeping the potential of the scanning probe microscope tip ($V_t = 0$ B) as well as the back-gate voltage (V_{BG}) constant. The conductance of the wire during the scan was measured in a two-terminal circuit by using a standard lock-in technique. The tip to SiO_2 surface distance chosen for the scanning process was $h_{tip} = 250$ nm. During SGM scans and linear magnetotransport measurements a driving AC signal with an amplitude of $I_{AC} = 0.8$ nA at a frequency of 231 Hz was applied to the source contact keeping drain contact grounded while the voltage was measured by a differential amplifier. External magnetic field was directed perpendicular to the wire axis and Si substrate surface.

3. EXPERIMENTAL RESULTS

In Fig. 2 the dependence of conductance (R^{-1}) of the nanowire as a function of back gate voltage V_{BG} is presented.

The overall linear dependence of conductance on back gate voltage (carrier density) is typical for Si-doped InAs nanowires [15]. Non-regular fluctuations are universal conductance fluctuations (UCF) which arise because the phase coherence length in InAs is comparable to the length of the wire. The magnified low back gate section of $R^{-1}(V_{BG})$ curve is shown in the top-left inset of Fig. 2. Additionally to the UCF, there are oscillations with period of $\Delta V_{BG} = 36$ mV, marked with blue oval. These oscillations come from the residual Coulomb

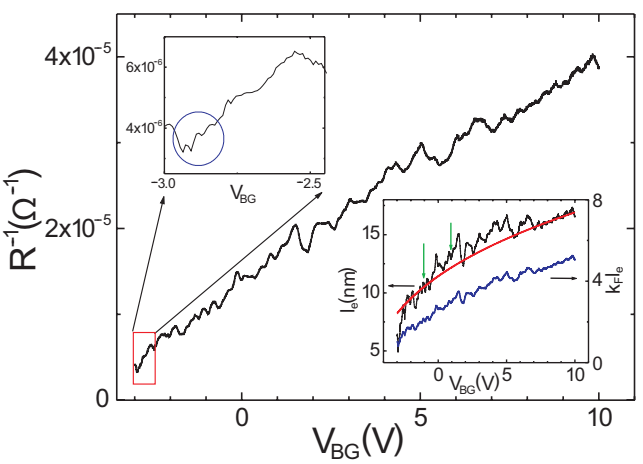

Fig. 2. (In color online) Conductance R^{-1} of the nanowire versus back gate voltage V_{BG}. Non-regular oscillations come from universal conductance fluctuations. The upper-left insert shows the dependence of the conductance on the back gate voltage in the range indicated by the dashed frame in the Figure. Small period oscillations within the range marked with blue circle come from residual Coulomb blockade of the quantum dot positioned in the mid part of the nanowire (see main text for details). The lower-right insert presents the elastic scattering length as a function of the back gate voltage (black curve, left scale). Blue curve in the insert shows the dependence of $k_F l_e$ on the back gate voltage (right scale). Two green arrows point to $V_{BG} = -1$ V and $V_{BG} = 1$ V.

blockade of a quantum dot positioned in the mid of the nanowire [18].

According to finite element calculations of the capacitance of the nanowire [19], the specific capacitance of our sample is $c_s \simeq 80$ pF/m.Thus, it is possible to calculate the carrier density of the nanowire within simple capacitance approximation as a function of the back gate voltage

$$n_e = \frac{c_s(V_{BG} - V_{Th})}{\pi e (d_{wire}/2)^2},$$

where $V_{Th} = -5.2$ V is the threshold voltage, and the elastic mean free path from Drude formula [20] is

$$l_e = \frac{h l_{wire}}{2\pi^2 e^2 R (d_{wire}/2)^2} \left(\frac{3\pi^2}{n_e^2}\right)^{1/3}.$$

The low-right inset in Fig. 2 shows the dependencies of l_e (black curve, left scale) and $l_e k_F$ (blue curve, right scale) on back-gate voltage, here $k_F = (3\pi^2 n_e)^{1/3}$ is the Fermi vector. The two green arrows on the inset at voltages $V_{BG} = -1$ V and 1 V show that the total change in both the magnitude of l_e and $l_e k_F$ is only 25–30% when V_{BG} increases from –1V to 1V.

The results of SGM mapping of the nanowire are presented in Figs. 3-8. Each figure demonstrates the evolution of the scanning results due to weak variation of the back gate voltage with a step of 10 mV (Figures a) to f)), and applied external magnetic field ($B = 0.1$, 0.2, 0.3, 0.5, 1 and 2 T, Figures g) to l)) for six back gate voltages, i.e., $V_{BG} = -3$, -2.1, -1, 1, 4 and 10 V, respectively. The step of V_{BG} was chosen to exceed correlation back gate voltage $V_{cBG} = hd/el_\phi^2 < 5$ mV for all applied V_{BG}, here D is the diffusion coefficient.

Mapping results of the SGM scanning in the vicinity of $V_{BG} = -3$ V presented in Fig. 3 demonstrate quite complex structure typical for nanowires or nanotubes with a number of the blocking barriers of different opacity [21]. The key feature of scans in Fig. 3 is well defined concentric ovals, see Figs. 3f) and 3l) for example. The presence and the position of such ovals means the formation of the quantum dot in the mid-section of the nanowire and ovals are the result of the Coulomb blockade realized in this dot [21]. The period of Coulomb blockade oscillations of $\Delta V_{BG} = 36$ mV allows to estimate the length of electronic system of this quantum dot $l_{dot} \simeq e / c_s \Delta V_{BG} \simeq 60$ nm. Taking into account the lengths of possible depletion zones of around ≈ 100 nm (this value is comparable to the silicone oxide thickness), the distance between two strong blocking barriers forming this dot can be estimated as $l_{BB} \simeq 250$ nm. Thus, this quantum dot is positioned approximately in the center of the wire with barrier-to-barrier distance $l_{BB} \ll l_{wire}$. It means that the nanowire is divided into three sections. The Section I extends from the source contact to the first blocking barrier, the Section II is the quantum dot itself and the Section III lays between the second blocking barrier and the drain contact.

The scanning gate microscopy mapping performed in the vicinity of $V_{BG} = -2.1$ V is shown in Fig. 4. At this back gate voltage the SGM mapping results look still quite complex, see Fig. 4a), but they demonstrate a response from all three sections of the nanowire. Here equicapacitance ovals and circles are not resulted from the Coulomb blockade, because the shape of them changes dramatically with

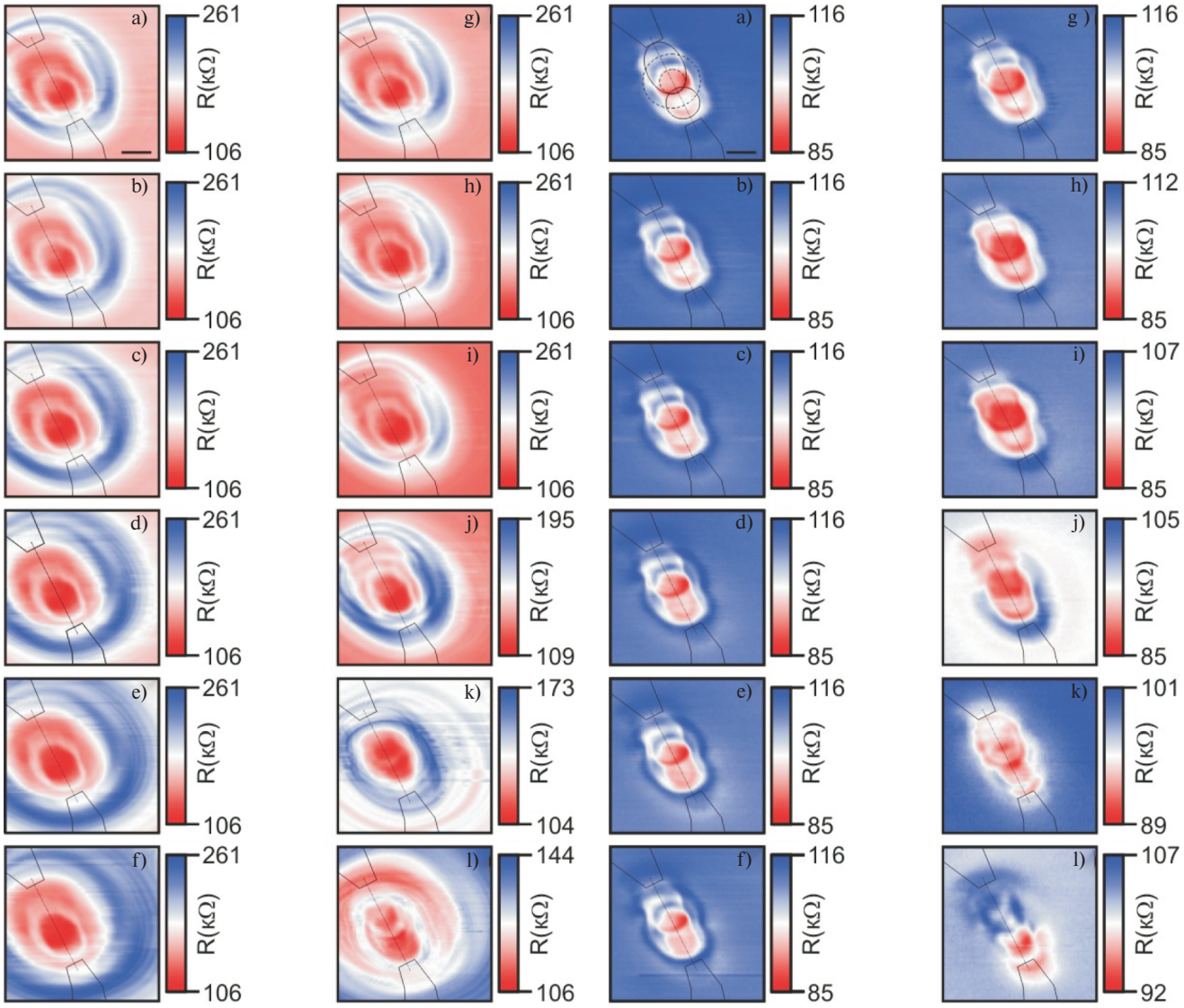

Fig. 3. (In color online) a)-f) Scanning gate microscopy maps of InAs nanowire carried out at zero magnetic field and in range of back gate voltages varied from V_{BG} = –3.00 V to –2.95 V with step of 10 mV, respectively. g)-l) Scanning gate microscopy maps gained at V_{BG} = –3.0 V and B = 0.1,0.2,0.3,0.5,2.0 T, respectively. Concentric circles are the sign of the Coulomb blockade in quantum dot positioned at the mid part of the nanowire. The scale bar in Figure a) corresponds to 1 μm. The scale and the area of scanning gate microscopy maps are the same for all scans. The black solid lines mark the borders of contact pads and the dotted line marks the axis of nanowire.

Fig. 4. (In color online) a)-f) Scanning gate microscopy maps of InAs nanowire obtained at zero magnetic field and in range of back gate voltages varied from V_{BG} = –2.10 V to –2.15 V, with step of 10 mV, respectively. g)-l) Scanning gate microscopy maps gained at V_{BG} = –2.1 V and B = 0.1, 0.2, 0.3, 0.5, 1.0 and 2.0 T respectively. The scale bar in Figure 4a) corresponds to 1 μm. The scale and the area of scanning gate microscopy maps are the same for all scans. The black solid lines mark the borders of contact pads and the dotted line marks the axis of nanowire. Ovals and circles of equicapacitance for all sections of the nanowire are shown in the Figure a). Two solid ovals relate to the Sections I and III, two dashed concentric circles mark equicapacitance curve for central quantum dot (Section II).

application of external magnetic field, see Figs. 4g)-4l). The equicapacitance ovals and circles in SGM data come from the alteration of the opacity of the blocking barriers or, probably, due to the variation of the density of states [2].

Fig. 5 shows the scanning gate microscopy mapping carried out in the vicinity of $V_{BG} = -1.0$ V. There is no clearly distinguished response from each of the nanowire segments. It is particularly noteworthy that the scanning results are virtually unchanged when both gate voltage and magnetic field are weakly varied, see Fig. 5a) – 5h). Increasing the applied magnetic field from $B = 0.5$ to 2 T leads to a significant change in the scanning results (Fig. 5j) – 5l)) similar to the experimental data shown in Fig. 4.

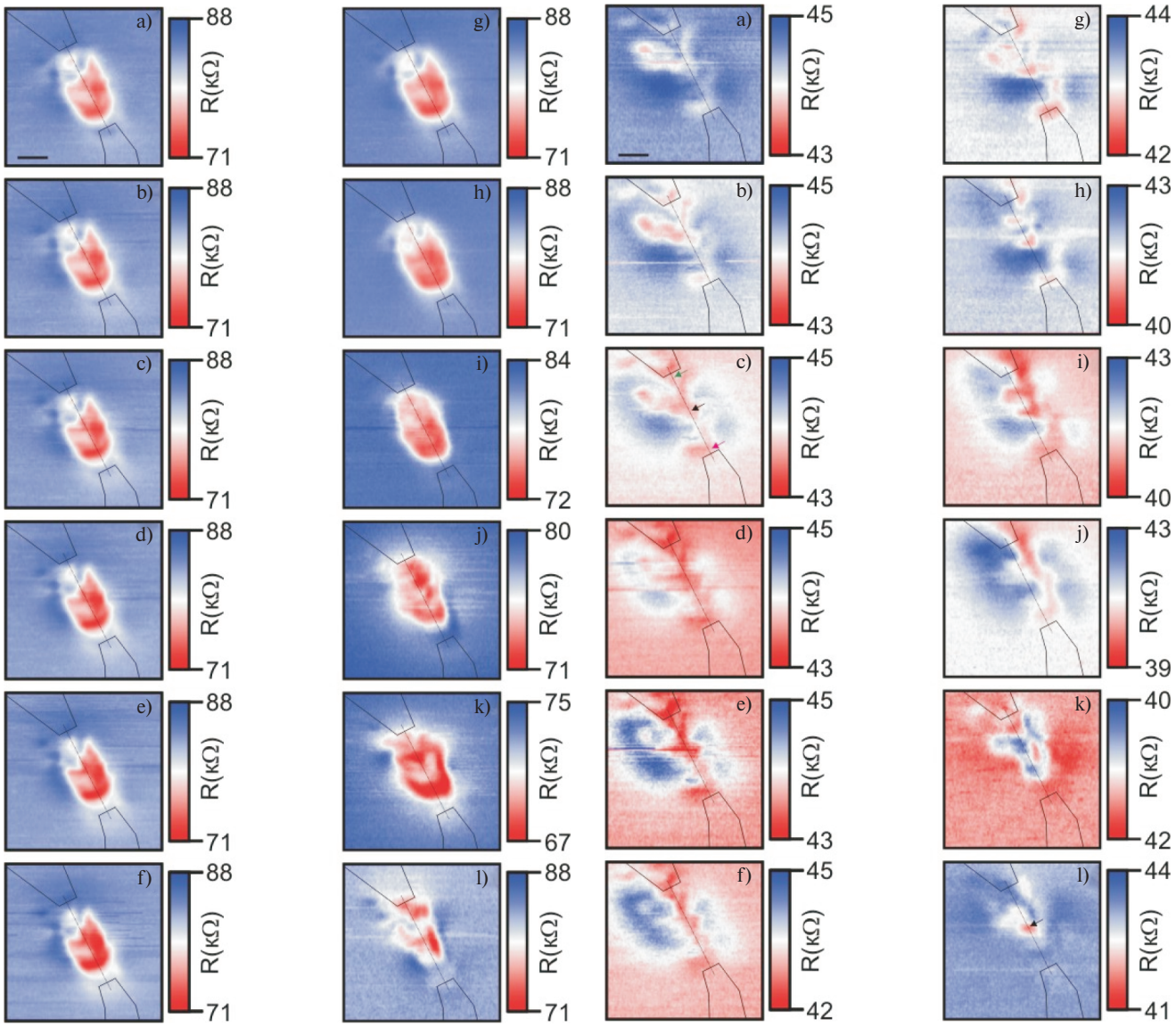

Fig. 5. (In color online) a)-f) Scanning gate microscopy maps of InAs nanowire made at zero magnetic field and in range of back gate voltages varied from V_{BG} = –1.00 V to –1.05 V, with step of 10 mV, respectively. g)-l) Scanning gate microscopy maps carried out at V_{BG} = –1.00 V and B = 0.1, 0.2, 0.3, 0.5, 1.0 and 2.0 T, respectively. The scale bar in Figure a) corresponds to 1 μm. The scale and the area of scanning gate microscopy maps are the same for all scans. The black solid lines mark the borders of contact pads and the dotted line marks the axis of nanowire.

Fig. 6. (In color online) a)-f) Scanning gate microscopy maps of InAs nanowire obtained at zero magnetic field and in range of back gate voltages varied from V_{BG} = 1.00 V to 1.05 V, with step of 10 mV, respectively. g)-l) Scanning gate microscopy maps gained at V_{BG} = 1.00 B and B = 0.1, 0.2, 0.3, 0.5, 1.0 and 2.0 T, respectively The scale bar in Fig. 6a) corresponds to 1 μm. The scale and the area of scanning gate microscopy maps are the same for all scans. The black solid lines mark the borders of contact pads and the dotted line marks the axis of nanowire. Arrows in Figure c) point to the positions of all potential barriers. The arrow in Figure I) points to the position of the central double barrier

The scanning gate microscopy mapping done in the vicinity of V_{BG} = 1.0 is presented in Fig. 6. Both the variation of back gate voltage and the magnetic field as small as 0.1 T alter the SGM mapping pictures. The smallest scale features of SGM scans have the size of 250 –300 nm. This size is comparable to the tip to SiO_2 surface distance and it is the spatial resolution of the current experimental setup [22]. Three well-defined resistance minima are visible in scans and marked with arrows in Fig. 6c). As it has been estimated previously, the distance between two barriers forming the central quantum dot at V_{BG} = –3 V is 250 nm, and each of the barrier cannot be resolved separately, so they are visualized

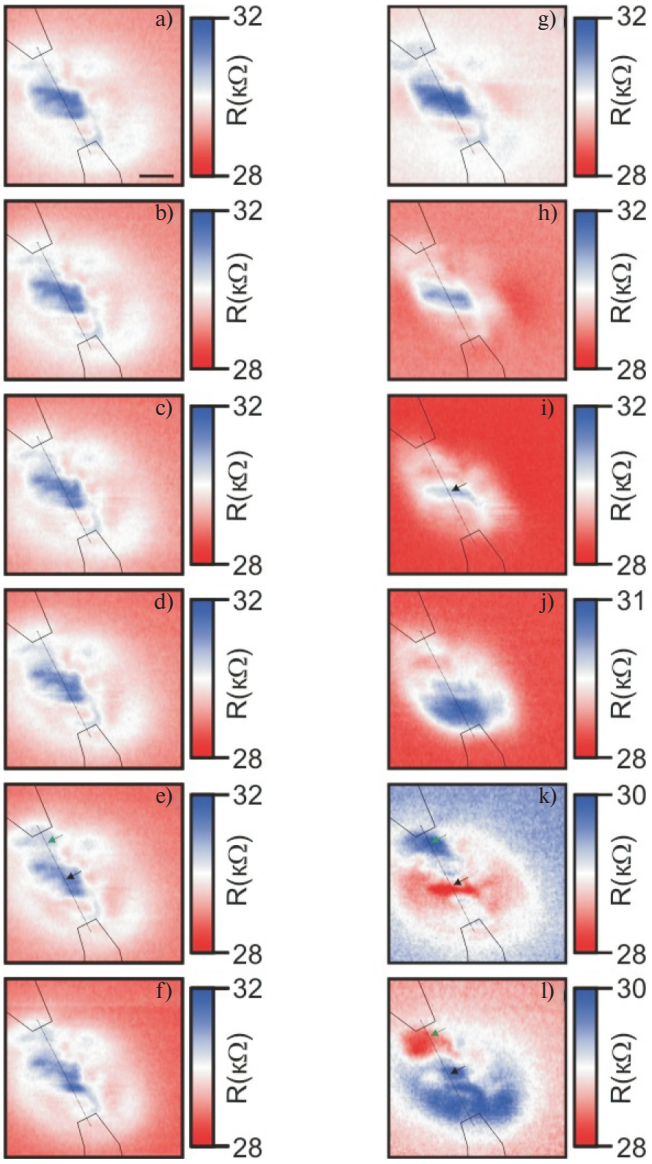

Fig. 7. (In color online) a)-f) Scanning gate microscopy maps of InAs nanowire carried out at zero magnetic field and in range of back gate voltages varied from V_{BG} = 4.00 V to 4.05 V, with step of 10 mV, respectively. g)-l) Scanning gate microscopy maps performed at V_{BG} = 4.00 and B = 0.1, 0.2, 0.3, 0.5, 1.0 and 2.0 T, respectively. The scale bar in Figure a) corresponds to 1 μm. The scale and the area of scanning gate microscopy maps are the same for all scans. The black solid lines mark the borders of contact pads and the dotted line marks the axis of nanowire. The black arrows point to the position of the central double barrier and the green ones point to barrier positioned close to the drain contact.

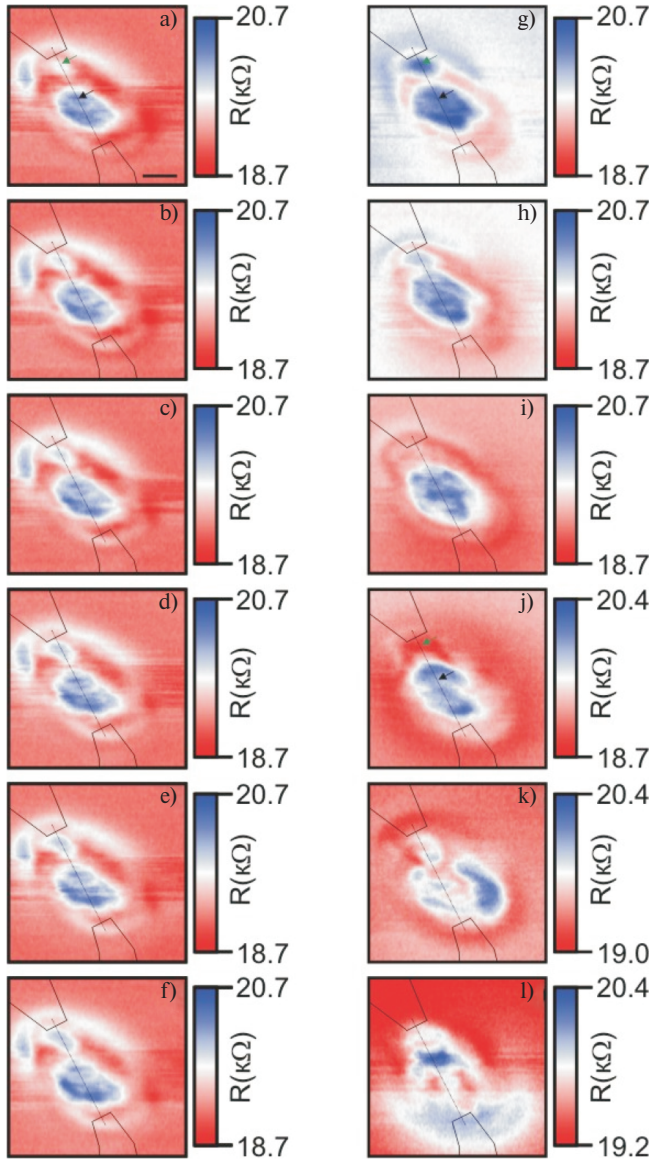

Fig. 8. (In color online) a)-f) Scanning gate microscopy maps of InAs nanowire obtained at zero magnetic field and in range of back gate voltages varied from V_{BG} = 10.00 V to 9.95 V, with step of 10 mV. g)-l) Scanning gate microscopy maps carried out at V_{BG} = 10.00 V and B = 0.1, 0.2, 0.3, 0.5, 1.0 and 2.0 T, respectively. The scale bar in Figure a) corresponds to 1 μm. The scale and the area of scanning gate microscopy maps are the same for all scans. The black solid lines mark the borders of contact pads and the dotted line marks the axis of nanowire. The black arrows point to the position of the central double barrier and the green ones point to barrier positioned close to the drain contact.

as a single one. Thus, these three minima are related to the source contact barrier, quantum dot double barrier, and the drain contact barrier. The positions of them are stable against variation of V_{BG} (Figs. 6a) -6f)). The double barrier sign (the red spot marked with black arrow) is visible even at SGM scan done at B = 2 T, see Fig. 6l). The scans shown in Fig. 6 additionally confirm the position of the quantum dot allocated from SGM mapping, see Fig. 4.

The SGM mapping done in the vicinity of V_{BG} = 4.0 and 10 V is shown in Fig. 7 and 8, respectively. These scans demonstrate the interplay

of the features come from UCF which vary their positions and the residual impact of the blocking barriers on the wire conductivity. It is worth noting that some minor influence of these barriers positions in SGM scans remains both at $V_{BG} = 4$ V(Fig. 7i)) and at $V_{BG} = 10$ V (fig. 8 *a*). (Fig. 8a)). This behavior of blocking barrier influence on SGM mapping is the same as observed in InN nanowires previously.

Figure 9 shows the dependence of the wire conductance (R^{-1}) on magnetic field measured at $V_{BG} = -3, -2, -1, 1, 4, 10$ V.

Curves, except one measured at $V_{BG} = 10$ V are shifted for clarity. Non-regular reproducible oscillations are UCF. The peak in conductivity around $V_{BG} = 10$ V comes from weak antilocalisation quantum correction due to spin-orbit interaction in the InAs. This transition from weak anilocalization to localization with decreasing the carrier concentration is typical for InAs nanowires [23-28].

The spectra of universal conductivity fluctuations, which are obtained from the experimental data of Fig. 9, are shown in Fig. 10.

The top panel of Fig. 10 shows universal conductance fluctuations spectra calculated from $R^{-1}(B)$ data measured at $V_{BG} = -3$, -2 and -1 V, and on the bottom at $V_{BG} = 1, 4$ and 10 B. The significant suppression of the spectrum at $1/B > 1$ T^{-1} for the spectra shown in the top panel of Fig. 10 is clearly visible.

Dependences of the normalised correlator $F(\Delta B) / F(0)$, calculated for the dependencies $R^{-1}(B)$, measured at $V_{BG} = -3, -2, -1, 1, 4$ and 10 V, are shown in Figure 11.

The smallest value of the correlation magnetic field of $B_c = 0.11$ T, which is obtained from experimental data measured at $V_{BG} = 10$ V and the corresponding electron phase failure length can be obtained and the corresponding electron phase length $l_\phi = 200$ nm can be obtained. This value is within the range from 200 to 500 nmobtained in nanowires InAs previously [23-30]. Significant increase of l_ϕ at higher carrier concentrations was also previously observed in [23, 24, 25]. When calculating the correlator $F(\Delta B) / F(0)$ were used $R^{-1}(V_{BG})$ data ranging from $B = 0.65$ to 7.0 T, to exclude the influence of quantum corrections to conductivity in the region of small magnetic fields.

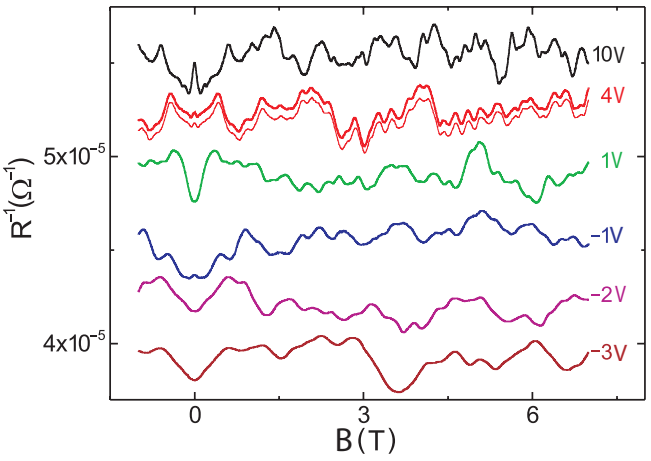

Fig. 9. (In color online) Magnetic field dependencies of the conductance of the nanowire (R^{-1}) measured in the range of magnetic fields from –1 T to 7 T and at different back gate voltages as indicated in Figure. Thin red curve (shifted for clarity) denotes the data obtained at $V_{BG} = 4$ V ramping external magnetic field down from 7 to –1 T. All other measurements were carried out at field reversal from the –1 to 7 T

Dependences of correlator variation $\Delta F(\Delta B) = F(\Delta B) - F(0)$ in a double logarithmic scale for $V_{BG} = -3, -2, -1, 1, 4$ and 10 V are shown in Figure 12.

The two straight lines show the slopes of the dependence ΔB^γ for two values $\gamma = 1.5$ (red line) and $\gamma = 2.0$ (black line).

Dependences of normalised differential resistance $(dV/dI)/(dV/dI(0))$ as a function of driving current, obtained at $V_{BG} = -3, -2, -1$ and 1 V are shown in Figure 13.

The dots on the curves mark the current values at which the $eV_{SD} = k_B T$. A distinctly nonlinear behaviour of the obtained dependencies is observed only at $V_{BG} = -3$ and -2 V. The experiment was performed at $B = 0.65$ T in order to exclude the influence of quantum corrections.

4. DISCUSSION

Transitions from Coulomb blockade to Fabri-Perot interference in ballistic one-dimensional and quasi-one- dimensional systems were recently observed and discussed in detail in [31,32]. In inhomogeneous diffusive quasi-one-dimensional systems, the transport phenomena are more complex. Presented data help to illustrate relevant transport regimes focusing on their peculiarities in magnetotransport data and the SGM mapping results obtained in the same run.

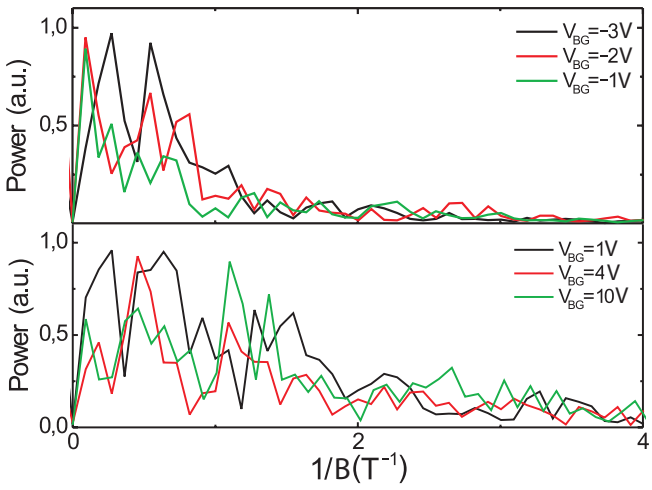

Fig. 10. (In color online) Top panel is power spectra of magnetoconductance for $V_{BG} = -3$, -2 and -1 V, see Fig. 9. Bottom panel is power spectra of magnetoconductance for $V_{BG} = 1$, 4 and 10 V, see Fig. 9. The significant suppression of all spectra for $1/B > 1$ T^{-1} presented in the top panel is clearly visible.

The doped InAs nanowire was chosen because of its homogeneous radial carrier density [15]. Thus, any influence on the transport resulted from cylindrical shape of the electronic system [33] is minor.

As noted earlier, the dependence of $R^{-1}(V_{BG})$ (fig. 2) and the data measured by the SGM technique at $V_{BG} = -3$ V (Fig. 3), allow us to determine the location and size of the quantum dot that is formed in the centre of the nanowire. The value of B_c, obtained from the experimental results presented in Fig. 11, confirms that loops with small area play the main role (90×50 nm^2) [34]. The transport at this value of the backgate voltage is non-linear, see Fig. 13.

InAs nanowires containing weak links (or fluctuations of the surface potential) tend to be divided into several quantum dots demonstrating the Coulomb blockade at low back gate voltages. This behavior is rather common and has been investigated in number of papers [18,35,36]. In case of more than one quantum dot containing in the wire, the correct interpretation of the observed Coulomb blockade diamonds is rather cumbersome. Nevertheless, as it has been shown for a simple case (two quantum dots), a charged AFM tip could help to associate a certain ladder of diamonds to a certain dot in the nanowire [35].

It should be noted that the experimental data obtained in Fig. 3 cannot be explained by the modulation of barrier transparency in the near-contact regions. In fact, some change in the sample conductivity due to the above effect can be observed, for example, in nanowires InN [3]. In this work, it was demonstrated that a closely spaced atomic force microscope tip can change the transparency of potential barriers at metal-semiconductor interfaces. However, the result of scanning by the SGM technique would have to result in two series of circles or ovals with centres located above the potential barriers, which is significantly different from the experimental results presented in Fig. 3, in which the centre of the concentric ovals is located near the centre

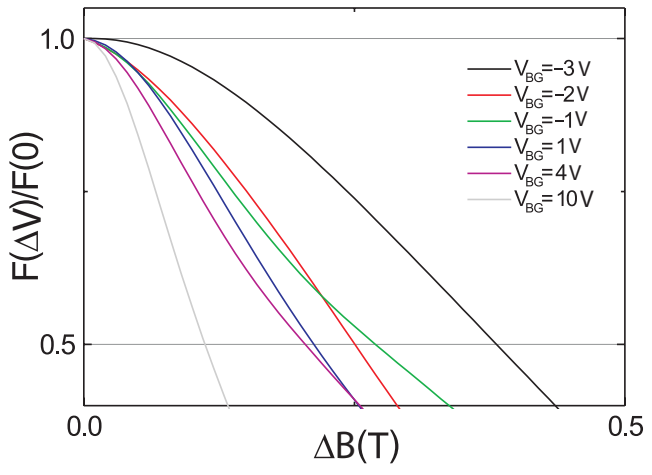

Fig. 11. (In colour online) Normalised dependencies of the correlation function $F(\Delta B) / F(0)$, calculated using the measured magnetic conductivity data presented in Fig. 9 for six different values of the back gate voltage

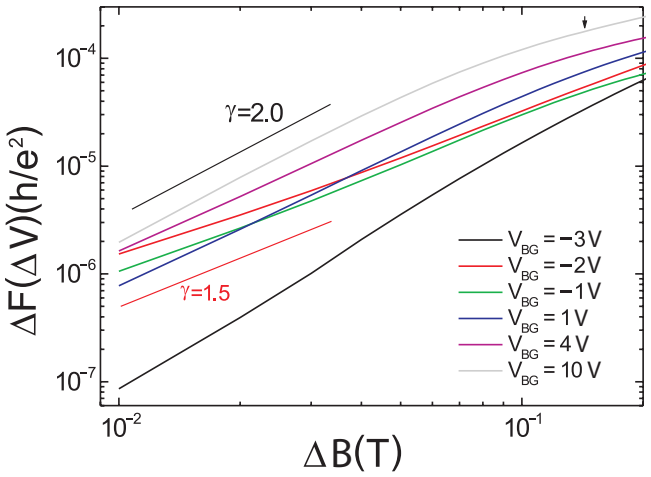

Fig. 12. (In colour online) Variation of the correlation function at six different boack gate voltages. The red and black straight lines correspond to two values of degree $\gamma = 1.5$ and 2.0. The arrow marks the value B_c for $V_{BG} = 10$ V

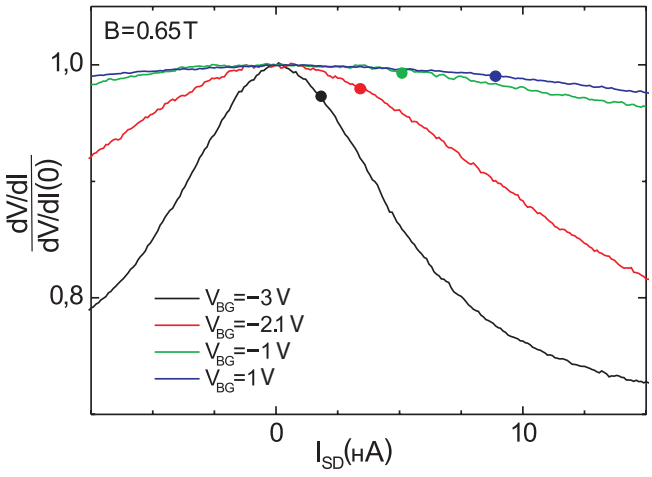

Fig. 13. (In colour online) a) Normalised differential resistance $(dV/dI)\,/\,(dV/dI(0))$ as a function of current (I_{SD}), measured at $V_{BG} = -3$, -2, -1 and 1 V. The dots on each curve mark the magnitude of the current at which the $eU_{SD} = k_BT$. Measurements were carried out in a magnetic field $B = 0.65$ T

of the nanowire, i.e. at a significant distance from the contact pads and the corresponding interfaces.

By increasing the carrier density concentration $V_{BG} = -2$ V, we transfer the system to non-linear resonant regime (see Fig. 13). In this regime, the strongest resonant scatterers (blocking barriers) define three quasi-localized states formed in corresponding Sections of wire. Maps obtained with the SGM technique depend weakly on variation of the back gate voltage and application of the small magnetic field, see Fig. 4. New energy scale of the order of 100 meV is the characteristic energy of variation of opacity of the blocking barriers and fluctuation of the density of states. The contribution from small area loops is dominant, see Fig. 11.

Further increase of the carrier concentration ($V_{BG} = -1$ B) gives rise to the reduced influence of the blocking barriers. Transport becomes linear, see Fig. 13. The data obtained by the SGM technique can no longer determine the number of segments into which the nanowire is split. It should also be noted that, despite the reduced influence of resonant scatterers, there is still a new energy scale in the system of 100 mV, and the results of the SGM scanning technique, as well as at $V_{BG} = -2$ V, depend weakly on the variation of the voltage on the bottom gate and the applied external magnetic field, see Fig. 5. The main contribution continues to be made by small area loops, i.e. segments with a characteristic length of 50 –100 nm. As mentioned above, the spatial resolution of the SGM technique in the presented experiment is 250 –300 nm, i.e., it is not possible to visualise each individual resonant scatterer.

At $V_{BG} = 1$ V we observe important changes in the SGM scans. The SGM mapping results (Fig. 6) become sensitive to the small (10 mV) increase of the back gate voltage as well as to application of the small ($B = 0.1$ T) external magnetic field. This behaviour of the electronic system was found previously in undoped nanowires InAs [37], it can be identified as a regime of practically homogeneous diffuse transport with essentially suppressed role of resonant scatterers. Additionally, the spectrum of the UCF extends to the higher frequencies (Fig. 10, bottom panel). This spectrum extension can be used as an additional indicator of the observed transition. Transport is linear as shown in Fig. 13.

Further increase of the back gate voltage results in even more homogeneous transport according to SGM data (Figs. 7 and 8) with wide spectra of UCF (Fig. 10, bottom panel). At $V_{BG} = 10$ V the correlation field B_c has reached the value related to the phase coherence length of 200 nm. It is worth noting while the value of B_c varies for less than 25% from $V_{BG} = -2$ to 4 V the Fermi velocity doubles. This artificial overestimation of the measured value B_c means a significant underestimation of the phase failure length due to strong wire segmentation at the $V_{BG} = -2$ and -1 V and partial segmentation at $V_{BG} = 1$ and 4 V ($\gamma(V_{BG} = 4\text{B}) = 1.71 < 2$).

Lightly doped wires InAs are not optimal objects for investigation of the behaviour of resonant scatterers using the SGM technique due to the presence of additional undulations introduced by USF in the scanning results at $V_{BG} \geqslant 1$ V. Nanowires with significantly higher density of states, such as InN, are more favoured targets [3]. In this case, the presence of a charged atomic force microscope tip does not result in additional undulation due to USF, visualising only resonant scatterers. Despite this, the data presented in Figs. 6 - 9 allow us to trace the changing response of the resonant blocking barriers with both increasing bottom gate voltage and changing external magnetic field, focusing mainly on the behaviour of the central double barrier (marked with a black arrow on the experimental scan data) and the barrier in the near-contact region of the drain (marked with a green arrow).

In Fig. 6(c) all three main barriers are visualised and marked with arrows. A key feature of resonant

scatterers is that when they are fixed in position, the proximity of the charged tip of an atomic force microscope can change the sign of the response as the bottom gate voltage changes (E_F), and at changing the strength of the external magnetic field [3, 20]. Let us trace both these features on the example of experimental data obtained using the SGM technique.

Changing the sign of response on AFM tip with variation of back gate voltages is presented in Fig. 6(c) and Fig. 7(e). While the tip decreases the resistance of the resonant scatterers at $V_{BG} = 1$ V, it rises the resistance at $V_{BG} = 4$ V. A similar change in the sign of the response when the magnetic field is changed is shown in Fig. 7 (k) and (l). Experimental data were obtained at the voltage on the back gate $V_{BG} = 4$ B and $B = 1$ and 2 T respectively. The scan results clearly show that the resistance of the barrier near the drain contact grows as the tip approaches at $B = 1$ T and decreases at $B = 2$ T. The response behaviour of the central double barrier is exactly the opposite, i.e. its resistance decreases at $B = 1$ T and grows at $B = 2$ T, see Fig. 7 (k, l) . The change of the sign of the response of resonant barriers occurs at a characteristic change of the magnetic field of the order of lT. This behaviour is consistent with the observed stability of the scanning results using the SGM technique, namely, the stability of the results obtained when the magnitude of the external magnetic field is weakly varied at $V_{BG} = -2.1$ and -1 V, when resonant scatterers have a significant effect on the electronic transport of nanowires.

The transition from the linear resonant regime to more homogenous diffusive one occurs at back gate voltages between $V_{BG} = -1$ V and 1 V (see two arrows in the bottom-right inset of the Fig. 2). As it has been mentioned previously, no essential variations of l_e or $k_F l_e$ happen in this range of back gate voltages. Therefore, while the larger energy scale is present in the linear resonant regime, it is not clear at present, what is the correct criterion demonstrating this transition just from the $R^{-1}(V_{BG})$ dependence. The switch of the behavior of SGM mapping results can be considered as an undoubtful evidence of transition from linear resonant regime to more homogenous diffusive one. The sudden increase of the high frequency spectrum of UCF can be considered as an additional indicator of this transition.

The most significant feature in the obtained experimental results is the non-trivial behaviour of the exponent γ in $\Delta F(\Delta B) \propto \Delta B^{\gamma}$ as a function of the back gate voltage, see Fig. 12. This exponent is $\gamma = 2.1 \pm 0.1$ for Coulomb blockade regime when the transport is defined mostly by quantum dot. Then, the value of exponent drops to values close to $\gamma = 1.4$ in non-linear and linear resonant scattering regimes, see Table 1. The transport depends strongly on resonant scatterers in the wire forming a set of quasilocalized states resulting in fractional Bownian motion of $R^{-1}(B)$ curve with dimensionality greater than one ($Dim = 2 - \gamma / 2 = 1.3$) [8, 12] for both non-linear and linear resonant regimes. The reason of weak variation of $\gamma = 1.4$ in this regime is presently not clear and might be the subject for further investigations. At ($V_{BG} \geqslant 1$ V), i.e., when the role of resonant scatterers is reduced, the value of the γ increases, reaching the standard value 2, see table 1.

Table 1. The dependence of the correlation field B_c and γ on back gate voltage

V_{BG}, V	B_c, T	γ
-3	0.48	2.10 ± 0.1
-2	0.25	1.38 ± 0.1
-1	0.27	1.42 ± 0.1
1	0.21	1.78 ± 0.1
4	0.21	1.71 ± 0.1
10	0.11	1.90 ± 0.1

According to the theoretical work of Altshuler-Gefen-Kamenev-Levitov (AGKL), three regimes should be realised at multiparticle localisation [38, 39]. The first of these occurs when the corresponding energy $k_B T$ is less than the characteristic energy at the quantum dot E_{QD} ($E_{QD}(V_{BG} = -3\text{ V}) = e\Delta V_{BG}\sqrt{g / \ln(g)} \sim 10$ meV, in this experiment it is the Coulomb blockade regime). In this regime, the one-electron states resemble the true many-electron states. The normalised condactance of the central quantum dot in this case is equal to $g = h/e^2 R_{QD} \sim 1$. In intermediate mode $k_B T < E_{Th,seg} \approx 1.7$ meV at $V_{BG} = -1$ the quasiparticle states have the form of fractals and are not ergodic [38, 39]. In this case $E_{Th,seg} = hD/l_{seg}^2$ – Thouless

energy of a typical wire segment formed by resonant scatterers.

The fractal structure of the wave functions and the general non-ergodic behaviour of the system in the intermediate state described by AGKL can be considered as some analogy with resonant modes of electron transport with fractal dependence behaviour $R^{-1}(B)$ in this experiment. It should be noted that the length of the wave vector $\lambda_F \simeq 37$ nm at $V_{BG} = -1$ V, this means that the number of channels in the system is $N_{channel} \simeq \pi d_{wire}^2/\lambda_F^2 \simeq 24$, and the length of the localisation $l_{loc} \simeq N_{channel} l_e \simeq 240$ nm. This value is comparable to l_{seg} and the phase coherence length at $V_{BG} = -1$ V:

$$l_\phi(V_{BG} = -1V) \simeq$$
$$\simeq \frac{k_F l_e(V_{BG} = -1V)}{(k_F l_e(V_{BG} = 10V))^{0.5}} \cdot 200 \approx 120\,\text{nm},$$

see Fig. 2, right inset, in case the phase coherence time depends weakly on the gate voltage. Thus, localisation in each individual segment appears to be possible ($l_\phi(V_{BG} = -1$ V$) \sim l_{loc}$). When the carrier concentration is further increased, when $k_B T$ becomes the largest scale of energy ($k_B T > E_{Th,wire} \sim 3$ μeV), the standard exponential damping of quasiparticles is established, $E_{Th,wire}$ is Thouless energy of the whole nanowire. This regime corresponds to the homogeneous diffuse regime in this paper.

Thus, as in AGKL theoretical picture, so in the current experiment there is a special regime with non-trivial behavior of the electronic system wave function or fractal Bownian motion of curve of dependence of conductance on magnetic field lying in between Coulomb blockade and homogeneous diffusion transport regimes. Let us discuss resonant transport regime, where the resonant scatterers play crucial role governing transport properties of InAs wire, in more details, focusing on the stability of SGM mapping data against small variation of magnetic field and additional possible nature of suppression of value of index $\gamma < 2$.

The stability of the scanning results using the SGM technique with respect to weak changes in the external magnetic field, see Figs. 4 and 5, can be qualitatively explained by the fact that the electron in the nanowire can cover an area significantly smaller than the $S_{diff} = d_{wire} l_\phi$. This situation is realised if the electron is blocked between two resonant scatterers (with characteristic distance between them l_{seg}) with the transparency of the relevant barriers $h/\tau_{rs} < h/\tau_\phi$, in this case τ_ϕ — is electron phase coherence time. If $l_{seg} < l_\phi$, then the corresponding value of the characteristic external magnetic field, at which the scanning result will change significantly, grows to the value of $B_C^* = \Phi_0/(d_{wire} l_{seg}) > \Phi_0/(d_{wire} l_\phi)$. This new scale by magnetic field (B_C^*) for the nanowire under study is 1 T and remains virtually unchanged for blocking barriers up to $V_{BG} = 4$ V, see Figs. 7(k) and 7(l).

The opacity of resonant scatterers depends both on the Fermi energy and the magnetic field, and besides defining the new scales in values of the magnetic field and the energy, the confinement of electrons made by them originates one very important issue. In the case of homogeneous diffusive transport, as it has been mentioned previously, the size of the area that electron sweeps to loose its phase is $S_{diff} = d_{wire} l_\phi$. This value does not depend on the magnetic field. In the case of Coulomb blockade regime, if the size of the dot (l_{dot}) is smaller than l_ϕ, the value of related area is $S_{Coulomb} = d_{wire} l_{dot}$. This value does not depend on the magnetic field as well. If resonant scatterers play an essential role in the transport, the situation is different as from the homogeneous diffusion transport, so from the Coulomb blockade regime, i.e. due to the variation of opacity of resonant blocking barriers with magnetic field, the size of the area for a certain electron $d_{wire} l_{seg} = S_{seg}(B)$ becomes a function of the magnetic field. Probably, the alteration of the area size that electron can sweep with magnetic field can be the reason why the value of index γ is less than 2. With increasing the back gate voltage the role of resonant scatterers diminishes and the value of $S_{seg}(B)$ is equal to S_{diff} and becomes constant. Similarly, when decreasing V_{BG} value of $S_{seg}(B)$ decreases to $S_{Coulomb}$ and is no longer dependent on B. As a result, the value of γ returns to its default value equal to 2 in both cases.

It should be noted that it is not possible to exclude the possibility of transition from the Coulomb blockade regime directly to the regime of homogeneous diffuse transport. However, this work shows the transition with intermediate modes of transport, demonstrating both peculiarities in the results of scanning by SGM technique and non-trivial

behaviour of dependence R^{-1} (B) with the dimension of Brownian motion $Dim > 1$.

There are quite a number of theoretical papers in which quasi-localized states formed by resonant scatterers are considered as a possible origin of formation of the observed fractional Bownian motion of dependence of conductance on magnetic field in the *intermediate regime* [40-42]. However, there have been no clear experimental evidences or visualizations of such kind of states. Here we show as the SGM mapping scans visualize them and hence the fractional Bownian motion they initiate.

5. CONCLUSION

We performed the low temperature measurements of the magnetotransport in doped InAs nanowire in the presence of a charged tip of an atomic force microscope serving as a mobile gate. By varying the carrier concentration, the system under investigation passes through four transport regimes from Coulomb blockade to homogeneous diffusive transport. Fractional Bownian motion of dependence of conductance on magnetic field is observed in non-linear and linear resonant transport regimes. Key experiments for demonstration of transition from the linear resonant transport regime to the diffusive one are presented. The experimental results are in general agreement with the theoretical model proposed by AGKL.

ACKNOWLEDGEMENTS

The authors would like to thank Chrisian Blömers for samples preparation and Raffaella Calarco for nanowire growth. This work is supported by the RSF grant 23-22-00141, https://rscf.ru/project/23-22-00141/.

REFERENCES

1. S. Datta, “Electronic transport in mesoscopic systems”, (Cambridge University Press, 1995).
2. B.L. Altshuler and A.G. Aronov in “Electron-Electron Interactions in Disordered Conductors”, Ed. by A.J. Efros and M. Pollack (Elsevier Science, North-Holland, 1985).
3. A.A. Zhukov, JETP **134,** 95-102 (2022).
4. Y. Imry, “Introduction to Mesoscopic Physics” (Oxford University Press, Oxford 1997).
5. B.L . Altshuler, Pisma Zh. Eksp. Teor. Fiz. **41,**530-533 (1985); JETP Lett. **41,** 648-651 (1985).
6. P.A. Lee, A. D. Stone and H. Fukuyama, Phys. Rev. B **35,** 1039-70 (1987).
7. C.W.J. Beenakker and H. van Houten, Phys. Rev. B **37,** 6544 (1988).
8. R. Ketzmerick, Phys. Rev. B **54,** 10841 (1996).
9. B.B. Mandelbrot, «The Fractal Geometry of Nature» (Freeman, San Francisco, 1982).
10. M. Jannsen, International Journal of Modern Physics B **08,** 943-984 (1994).
11. F. Evers and A.D. Mirlin, Rev. Mod. Phys. **80,** 1355 (2008).
12. H. Hegger, B. Huckestein, K. Hecker, M. Janssen, A. Freimuth, G. Reckziegel, and R. Tuzinski, Phys. Rev. Lett. **77,** 3885 (1996).
13. C.A. Marlow, R.P. Taylor, T. P. Martin, B. C. Scannell, H. Linke, M.S. Fairbanks, G. D.R. Hall, I. Shorubalko, L. Samuelson, T.M. Fromhold, C. V. Brown, B. Hackens, S. Faniel, C. Gustin, V. Bayot, X. Wallart, S. Bollaert, and A. Cappy, Phys Rev B **73,** 195318 (2006).
14. K.R. Amin, S. S. Ray, N. Pal *et al.* , Commun Phys **1,** 1 (2018).
15. S. Wirths, K. Weis, A. Winden, K. Sladek, Ch. Volk, S. Alagha, T. E. Weirich, M. von der Ahe, H. Hardtdegen, H. Luth, N. Demarina, D. Grützmacher, and Th. Schapers, J. Appl. Phys. **110,** 053709 (2011).
16. M. Akabori, K. Sladek, H. Hardtdegen, Th. Schapers, and D. Grützmacher, J. Cryst. Growth **311, 3813 (2009).**
17. A.A. Zhukov, Instrum. Exp. Tech. **51,** 130-134 (2008).
18. K. Weis, St. Wirths, A. Winden, K. Sladek, H. Hardtdegen, H. Luth, D. Grützmacher, and Th. Schapers, Nanotechnology **25,** 135203 (2014).
19. O. Wunnicke, Appl. Phys. Lett. **89,** 083102 (2006).
20. V.F. Gantmakher, “Electrons and Disorder in Solids”, (Oxford University Press, 2005).
21. M.T. Woodside and P.L. McEuen, Science **296,** 1098 (2002).
22. A.A. Zhukov, Ch. Volk, A. Winden, H. Hardtdegen, and Th. Schapers, J. Phys. Condens. Matter **26,** 165304 (2014).
23. A.C. Bleszynski, F. A. Zwanenburg, R. M. Westervelt, A. L. Roest, E. P.A. M. Bakkers, and L.P. Kouwenhoven, Nano Lett. **7,** 2559-2562 (2005).
24. S. Dhara, H. S. Solanki, V. Singh, A. Narayanan, P. Chaudhari, M. Gokhale, A. Bhattacharya, and M.M. Deshmukh, Phys. Rev. B **79,** 121311(R) (2009).

25. P. Roulleau, T. Choi, S. Riedi, T. Heinzel, I. Shorubalko, T. Ihn, and K. Ensslin, Phys. Rev. B **81,** 155449 (2010).
26. Ch. Blomers, M. I. Lepsa, M. Luysberg, D. Grützmacher, H. Liith, and Th. Schapers, Nano Lett. 11, 3550-3556 (2011).
27. E.E. Boyd, K. Storm, L. Samuelson, and R.M. Westervelt, Nanotechnology **22,** 185201 (2011).
28. L.B. Wang, J. K. Guo, N. Kang, D. Pan, S. Li, D. Fan, J. Zhao, and H.Q. Xu, Appl. Phys. Lett. **106,** 173105 (2015).
29. K. Takase, Y. Ashikawa, G. Zhang, K. Tateno, and S. Sasaki, Scientific Reports **7,** 930 (2017).
30. D. Liang, J. Du, and X.P.A. Gao, Phys. Rev. B **81,** 153304 (2010).
31. A. Makarovski, J. Liu, and G. Finkelstein, Phys. Rev. Lett. **99,** 066801 (2007).
32. L.B. Wang, D. Pan, G. Y. Huang, J. Zhao, N. Kang, and H.Q. Xu, Nanotechnology **30,** 124001 (2019).
33. H. Luth, Ch. Blomers, Th. Richter, J. Wensorra, S. Estevez Hernandez, G. Petersen, M. Lepsa, Th. Schapers, M. Marso, M. Indlekofer, R. Calarco, R. Demarina, and D. Grutzmacher, Phys. Status Solidi C 7, 386-389 (2010).
34. H. Haucke *et al.*, Phys. Rev. B **41,** 12454 (1990).
35. **A.A.** Zhukov *et al.*, JETP **115,** 1062 (2012).
36. A.A. Zhukov *et al.*, JETP **116,** 138 (2013).
37. **A.A.** Zhukov, Ch. Volk, A. Winden, H. Hardtdegen, and Th. Schapers, J. Phys. Condens. Matter **26,** 165304 (2014).
38. B.L. Altshuler, Y. Gefen, A. Kamenev, and L.S. Levitov, Phys. Rev. Lett. **78,** 2803 (1997).
39. A.D. Mirlin and Y.V. Fyodorov, Phys. Rev. B **56,** 13393 (1997).
40. B.L. Altshuler, V. E. Kravtsov, and I.V. Lerner, JETP Lett. 45, 199 (1987).
41. B.A. Muzykantskii and D.E. Khmelnitskii, Phys. Rev. B **51,** 5480 (1995).
42. A.D. Mirlin, JETP Lett. **62,** 603 (1995).